Dynamics properties of xenon at high pressures: Hydrodynamic and nonhydrodynamic behavior

L. Letamendia, J. L. Cabanié, C. Vaucamps, and G. Nouchi
Centre de Physique Moléculaire Optique et Hertzienne, Université de Bordeaux I, 351 Cours de la Libération, 33405 Talence CEDEX, France

(Received 2 August 1990; revised manuscript received 1 May 1991)

We report experimental results of Rayleigh-Brillouin spectra of xenon along the isotherm $T_1=293.26$ K at high pressures, up to 130 atm. For this purpose we use the available measurements of thermodynamic and transport properties for the numerical simulation of the model. We clearly identify a pressure domain centered at the pressure $P_1=64$ atm corresponding to the critical density at T_1. In the pressure domain outside the pressure range defined by $P_1 \mp 25$ atm, the full Rayleigh-Brillouin spectra are described by hydrodynamic theory. Inside this pressure range, experimental spectra are only partially described by the model used, but nevertheless we confirm the existence of a diffusive mode partially detected by Cannell and Benedek [Phys. Rev. Lett. **25**, 1157 (1970)]. This mode reaches a maximum of intensity and width at half height for the pressure P_1. We discuss an explanation for the critical perturbation of the Brillouin line with this mode.

I. INTRODUCTION

Dynamics of atomic gases at low and moderate pressures have been studied by light-scattering techniques for many years [1–7]. Those works were essentially devoted to the determination of the domain of validity of hydrodynamic and kinetic theories [8].

Higher-pressure measurements of xenon dynamics were performed along the critical isochore both by light-beating spectroscopy (LBS) [9] and Rayleigh-Brillouin spectroscopy (RBS) [10] and the aim of those works was to explore the validity of the critical dynamic theories. The situation is not well known yet and if we follow the work of Sarid and Cannell [11] the Brillouin results of Xe remain unexplained in a large vicinity of the critical point. Otherwise, linewidth measurements of the Rayleigh line are well known close to the critical point and the usual critical behavior is obtained [9]. In a relatively large proximity of the critical point, there are few available results obtained by LBS and it can be noted that there is an important unresolved portion of the RBS, centered in the Rayleigh line [10].

In this paper we present results obtained with the light-scattering Rayleigh-Brillouin technique, along the isotherm corresponding to the temperature $T_1=293.26$ K and for pressures up to 130 atm. During the span of the pressure domain, the critical density is crossed for the pressure $P_1=64$ atm. The information obtained from those experiences can be divided in two groups. In the first one we put together all the results which follow the hydrodynamic regime, in the sense that those results agree with dynamics calculations developed with the hydrodynamic model [12]. A second group of results disagrees with the usual hydrodynamic theory [14] but we will try to analyze them with the help of the known dynamics behavior in the large vicinity of the critical point. Experimental results show two well-defined domains of pressure in regard to the dynamic properties, (a) the region outside the domain $40<P<90$ atm in which the hydrodynamic model describes the full Rayleigh-Brillouin spectrum and (b) the region where the pressure is contained in the domain $40<P<90$ atm in which only some of the properties are described in the framework of the hydrodynamic model. If we define $\Delta P=25$ atm, the pressure domain of nonhydrodynamic behavior is defined by $P=P_1\pm\Delta P$.

These kinds of results are not surprising if we look at the problem of critical phenomena. The evolution of the correlation length ξ at $\rho=\rho_C$, for the temperature T_1, using the usual expression $\xi=\xi_0\epsilon^{-\nu}$ where $\nu=0.63$ and $\epsilon=(T-T_c)/T_c$, leads to a value of $\xi=32$ Å and the value of its product by the wave vector q is $q\xi=0.064$. This value of $q\xi$ is smaller than the value given by Henry, Swinney, and Cummins [13] for the border of the hydrodynamic region, which is $q\xi\leq 0.2$; but it is not certain that the condition $q\xi\ll 1$ has been entirely satisfied. Cannell and Benedek had found in an earlier work [10] that a new diffusive mode can take place in the dynamic, near the critical density. The restrictions of their experimental setup do not let them know all the spectrum because with the loss of a great part of the central region of the spectrum it is impossible to analyze the full dynamical structure factor corresponding to the Rayleigh-Brillouin spectrum.

The entire Rayleigh-Brillouin spectrum is studied in this set of pressures, and the simultaneous determination of both the Brillouin and the Rayleigh lines permits us to obtain interesting results.

An important result of this work is the full evidence of a diffusion mode that reaches its maximum of intensity and half width at half height (HWHH) for ρ_C and is present only in the domain ΔP. That means that the central or Rayleigh line follows the hydrodynamic behavior $D_T q^2$ outside ΔP and inside this domain increases with P until P_1 and decreases probably until $D_T q^2$ after ΔP. When we reach the upper limit of ΔP, the resolution of

our experimental setup reaches its limit of resolution.

As we will see in the following sections, the Brillouin width has dramatic changes too in this domain, and its width increases from its hydrodynamic values as defined by formula (1) to a maximum reached at ρ_C. It decreases after that density until it reaches hydrodynamic values. That broadening of the Brillouin line has also been studied by several authors [3–5] along the critical isochore, but in this work we can evaluate a domain of pressures where we know the border of nonhydrodynamic behavior, for a given isotherm.

We evaluate carefully the thermodynamic and transport coefficients needed in the numerical simulations. The choice of those parameters and the brief description of the hydrodynamic theory is given in the next section. The description of the experimental setup and the experimental procedure are developed in Sec. III and the presentation of the results on the hydrodynamic regime and the discussion are in Sec. IV. Nonhydrodynamic results are given in Sec. V. Section VI is devoted to the comparison with previous works and the discussion of the results.

II. HYDRODYNAMIC THEORY AND DETERMINATION OF THE PARAMETERS

Thermal fluctuations of a one-component fluid are described with hydrodynamic equations that represent the conservation of mass, momentum, and energy [12]. Instead of the usual thermodynamic fluctuating variables corresponding to the pressure P and the temperature T, we use, for numerical simulation convenience, the variable defined for mixtures [14] $\varphi = T - (T_0 \alpha_T / \rho C_P) P$ where α_T is the thermal expansion coefficient, ρ the density, C_P the specific heat at constant pressure, and T_0 the temperature at equilibrium. With the usual Mountain variables and the last variable defined by $\Psi = \nabla \mathbf{v}$ where $\mathbf{v}$ is the mean speed of particles, we define the set of three variables needed for the description of the fluid.

The Fourier-Laplace transform of those equations can be represented as usual by the matrix equation,

$$(M + sI)V(q,s) = V(q,0)$$

where M and I are the hydrodynamic matrix and the unit matrix, respectively. $V(q,s)$ and $V(q,0)$ are column vectors corresponding to the variables φ, P, and Ψ and their initial condition values, respectively, and $s = i\omega$ where ω is the frequency.

The hydrodynamic matrix has the form

$$M = \begin{vmatrix} D_T q^2 & \dfrac{(\gamma-1)\chi_s D_T q^2}{\alpha_T C_P} & 0 \\ \dfrac{\alpha_T D_T q^2}{\chi_S} & (\gamma-1) D_T q^2 & \dfrac{iq}{\chi_S} \\ 0 & \dfrac{iq}{\rho} & bq^2 \end{vmatrix}$$

where $D_T = \lambda/\rho C_P$, $\gamma = C_P/C_V$, and $b = 4(\eta_S + \eta_V)/3\rho$.

The parameters η_S and η_V are the shear viscosity and volume viscosity, λ the thermal conductivity, χ_S the adiabatic compressibility, and q the wave vector under consideration defined by

$$q = \frac{4\pi n}{\lambda_0} \sin\frac{\theta}{2} .$$

Here, n is the index of refraction, θ the angle of diffusion, and λ_0 the wavelength of the laser radiation. The refractive index depends on the density and using the Clausius-Mossotti equation, we take into account that dependence in the calculation of the wave vector q. The value at ρ_C agrees with the value obtained elsewhere [9].

The fluctuating thermodynamic variables are coupled to the permittivity fluctuations $\delta\epsilon$ by

$$\delta\epsilon = (\epsilon - 1)\left[\frac{-\alpha'}{T_0}\varphi + \frac{\beta'}{\gamma P_0} P\right]$$

in which $\alpha' = (\delta\rho/\delta T)_P$ and $\beta' = \gamma P \chi_S$.

The scattered spectrum $I(q,\omega)$ is obtained by the relation

$$I(q,\omega) \propto \mathrm{Re}\langle \delta\epsilon(q,\omega)\delta\epsilon(q,0)\rangle$$

and the correlation function of the permittivity is expressed in terms of the correlation functions of the variables φ and P which can be evaluated with the help of the dynamic matrix M.

For the numerical simulation of the spectra we have to evaluate the transport coefficients and thermodynamic coefficient for all the terms of the hydrodynamic matrix M for each pressure which has been studied.

The viscosity measurements of Strumpf, Collins, and Pings [15] were used in the calculations. In Fig. 1 we have plotted the values of the viscosity corresponding to all the densities at the temperature T_1.

We use the thermal conductivity values of Trappeniers [16], plotted in Fig. 2 for all the needed densities at T_1.

There are available measurements of thermodynamic parameters by Habgood and Schneider [17] only in a small region of densities close to the critical point and measurements of Michels, Wassenaar, and Louwerse [18] in a large domain of densities but for temperatures higher

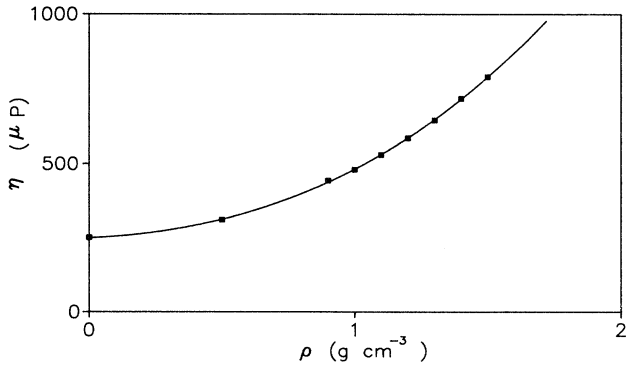

FIG. 1. Viscosity values of xenon vs studied densities for the temperature $T_1 = 293.26$ K after Strumpf, Collins, and Pings [15]. The values of the viscosity are given in micropoises.

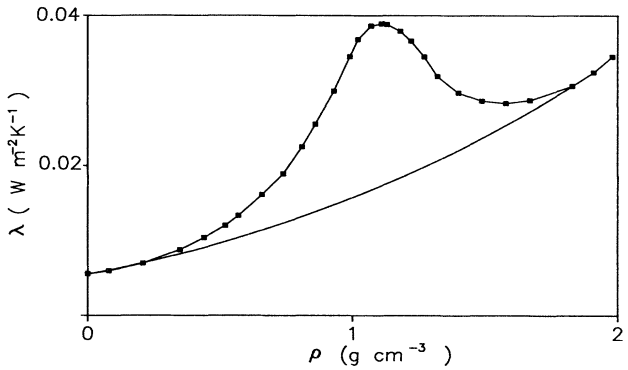

FIG. 2. Thermal conductivity values of xenon vs studied densities for the temperature T_1 after Trappeniers [16].

than T_1. Using all those available data we calculate an equation of state for the temperature T_1 for all the densities. This calculation was developed with a nonlinear mean square method and we evaluate the virial coefficients and their first-order and second-order derivatives required for the evaluation of all the thermodynamic properties.

This equation of state was calculated as an extension of a nine-virial-coefficient equation developed by Michels, Wassenaar, and Louwerse. The thermodynamic coefficients obtained with that equation are in agreement with known thermodynamic quantities such as C_P and C_V obtained by Habgood and Schneider and related quantities such as the sound speed V and specific-heat ratio γ obtained in light-scattering experiments by Swinney and Henry [9], Cannell and Benedek [10], and Cummins and Swinney [19] at ρ_C.

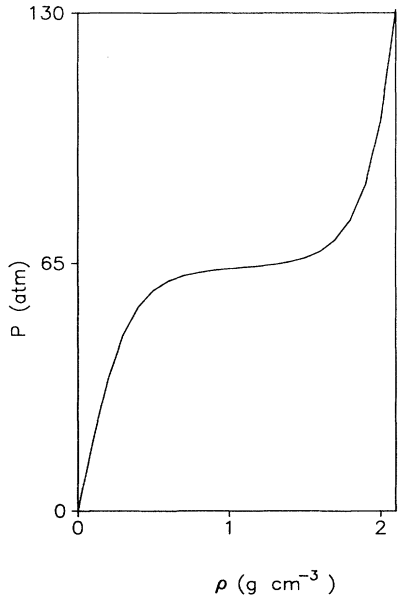

FIG. 3. Plot of pressure vs density virial state equation of xenon corresponding to T_1. See text for more details.

The equation of state is defined by

$$P=\rho k_B T \sum_{i=1}^{9} K_i \rho^{i-1}$$

where k_B is the Boltzmann constant and the quantities K_i are the virial coefficients.

In the Appendix we summarize the values of K_i, $K_i'=T\partial K_i/\partial T$, and $K_i''=T^2\partial^2 K_i/\partial T^2$ that correspond to the virial coefficient, the first derivative of the virial coefficients, and the second derivative of the virial coefficients, respectively. The behavior of P versus the density ρ is plotted in Fig. 3.

III. EXPERIMENTAL SETUP

We have developed an experimental setup for the Rayleigh-Brillouin light-scattering study of fluids and its essential characteristics will be presented here. The light beam is delivered by a 171 Spectra Physics argon laser and the monomode radiations we can use have wavelengths of 5145, 4785, and 4579 Å. The incident light is divided in two parts, (a) the first one with 90% of the intensity is the incident beam for the light beating experience itself and (b) the second one is needed for the alignment of optical devices, especially the Fabry-Pérot interferometer.

The gas is in a cell with arms that ensure spectra without detectable stray light. The scattered light is analyzed by a double-pass plan Fabry-Pérot (DPPFP) and its parallelism is obtained and maintained by an automatic device built in the laboratory [20]. This same device ensures the piezoelectrical scanning of the DPPFP and the typical finesse is better than 40. The usual free spectral range (FSR) for this work is 1785 MHz. The simultaneous determination of the apparatus function and the Rayleigh-Brillouin spectra allows us to make the convolution of a theoretical calculation. After dispersion by the DPPFP, the scattered light is collected by a photomultiplier and sent to a multichannel analyzer. These data can be stored in the memory of a computer for further processing or drawn by an (x,t) plotter.

All optical elements are over a granite table in order to be mechanically insulated from vibrations. Xenon gas of a purity of 99.99% is introduced in the cell using a cryopump cooled by liquid nitrogen. Pressure variation is obtained with the combination of increasing the amount of xenon by means of the cryopump and with the reduction of total volume of a cylindrical auxiliary container connected with the cell. The temperature stability is 0.1 °C.

IV. HYDRODYNAMIC RESULTS

The studied range of pressures is scanned starting from low pressures until reaching the higher pressure after having crossed the pressure corresponding to the critical density ρ_C. We have to note that for transport and thermodynamic properties there are perturbations due to the vicinity of the critical point and it is interesting to determine the domain of validity of the hydrodynamic model in such conditions. In this section we will give all the results predicted by the hydrodynamic theory which are in accordance with the experimental results. For this pur-

pose we will analyze the more important properties given usually by the Rayleigh-Brillouin spectra of a pure fluid. It is important to note that the full experimental spectra are in agreement with the calculated dynamic structure factor for a pressure domain outside a range of pressure defined by $40 < P < 90$ atm. But there are some properties connected with parts of the spectra which are in agreement with the hydrodynamic calculation inside this domain of pressure.

A. Landau-Placzek ratio

The ratio $I_C/2I_B$ of the total intensity of the Rayleigh or central line I_C and two times the total intensity of the Brillouin line I_B is called the Landau-Placzek ratio. That quantity can be evaluated from the experimental spectra and with the help of a relation of the ratio of the specific heat at constant pressure and volume γ, obtained for pure fluids in the calculation of the hydrodynamic model. This relation is defined by

$$\frac{I_C}{2I_B}=\gamma-1 .$$

The measurements of the intensity ratio are in good agreement with the γ values obtained from the measurements of Habgood and Schneider [17] and with the γ values obtained with the equation of state we have determined. We have to note that for the density $\rho=\rho_C$, we have a value compatible with the value obtained by Cannell and Benedek [10]. For us, those results mean that the evolution of the intensity ratio in that condition follows the hydrodynamic behavior. In Table I, we report some values of the experimental intensity ratio and values obtained by thermodynamic measurements.

TABLE I. Comparison between the measured values of the Landau-Placzek ratio $I_C/2I_B$ and the thermodynamic quantity $\gamma-1=(C_P-C_V)/C_V$ calculated with the C_P and C_V evaluated by thermodynamic measurements. See text for more details.

P (atm)	ρ (g cm^{-3})	$I_C/2I_B$	$\gamma-1$
11.2	0.06	0.68	0.67
20.41	0.11	0.70	0.71
30.2	0.17	0.80	0.81
40.99	0.25	1.1	1.12
50.36	0.35	2.0	1.99
55.18	0.43	3.4	3.42
61.06	0.64	14.0	13.90
63.0	0.86	35.0	35.10
64.0	1.11	53.0	53.0
65.0	1.35	31.0	31.16
66.1	1.47	21.0	21.40
69.93	1.67	11.0	11.34
80.17	1.85	6.0	5.83
89.6	1.93	4.0	4.04
100.0	1.99	3.2	3.15
120.6	2.07	2.4	2.37
127.2	2.09	2.2	2.21

B. The sound speed

In the hydrodynamic calculation of simple fluids, the sound speed is related with thermodynamic quantities and defined by the relation

$$v^2=(\rho\chi_S)^{-1} .$$

As expected by hydrodynamic calculation, v decreases when the density increases up to the critical density, and begins to increase after ρ_C, as shown in Fig. 4. In this plot it can be seen that the available thermodynamic data describe correctly the Brillouin-measured speed of sound. For the critical density the measured speed of sound is in accordance with the previous measurement along the critical isochore of Cannell and Benedek [10].

After the properties that can be described by the hydrodynamic model for all the studied pressures, there are some properties that follow the hydrodynamic regime only in a part of the studied domain of pressures. The sound attenuation that corresponds to the Brillouin width and the thermal relaxation that corresponds to the Rayleigh width are properties partially described in the hydrodynamic regime.

C. Rayleigh width

In the hydrodynamic regime the HWHH is described by

$$\Gamma_R=D_T q^2$$

where D_T is the thermodiffusivity defined in Sec. II. If we evaluate numerically that coefficient with the parameters λ, ρ, and C_P defined or calculated in Sec. II, the agreement between the calculated Γ_R and the measured HWHH is found only in the region of pressures outside $40 < P < 90$ atm.

D. Brillouin width

The value of the width at half height of the Brillouin line in the hydrodynamic calculation is Γ_B,

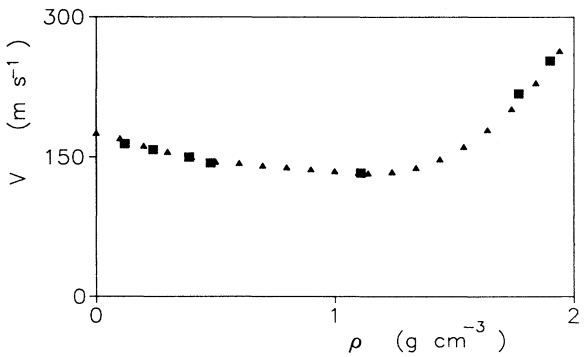

FIG. 4. Density dependence of the sound speed of xenon. Triangles represent the values deduced from the state equation and the squares correspond to experimental values.

$$\Gamma_B = \left[\frac{1}{\rho} \langle \tfrac{4}{3}\eta + \eta_B \rangle + \langle \gamma - 1 \rangle \frac{\lambda}{\rho C_P} \right] q^2 .$$

For the pressure domain outside $40 < P < 90$ atm the Brillouin width can be described without any bulk viscosity and the expression of Γ_B is correct with $\eta_B = 0$.

We can conclude that in this section we have presented the part of light-scattering studies of xenon along the isotherm T_1 that can be described in the framework of the hydrodynamic model of Mountain and Deutch [14]. For this purpose we have evaluated the transport and thermodynamic coefficients available for those conditions and computed all the spectra corresponding to the experimental conditions.

We find that the sound propagation and the Rayleigh-Brillouin intensity ratio are described, in the full experimental domain, by the hydrodynamic model. But for the sound attenuation and the thermal relaxation there are two pressure domains that can be roughly defined by $40 < P < 90$ atm where the hydrodynamic model does not describe the experimental results and the pressures outside this domain where those properties are in agreement with that model.

All the properties which depend on the thermodynamic coefficients are quite well described, that means a good agreement between thermodynamic measurements of Habgood and Schneider [17] or extrapolated values from Michels, Wassenaar, and Louwerse [18] and thermodynamic parameters obtained from the spectra using the hydrodynamic model.

As stated in the Introduction, maybe we are not too far from the limit of the hydrodynamic region and we are exploring the neighbor of the intermediate region as defined by Swinney and Henry [9]. As far as we know, in this region of pressure, we do not have multiple scattering because we are at a difference of temperature to the critical point T_c equal to $T - T_c = 3.45$ K large enough to avoid this kind of problem [21].

It is clear that the perturbation of the dynamics is due to the neighborhood of the critical point and for the description of this region we need to adopt a different point of view. The information we can get from the Rayleigh-Brillouin spectra depending on the thermodynamic properties is in quite good agreement with the thermodynamic parameters obtained independently by thermodynamic methods. The situation is different for the properties depending on the transport coefficients and in the following section we will present the results that do not follow the hydrodynamical behavior, trying to connect that fact with critical effects in a large domain of pressures.

V. NONHYDRODYNAMIC RESULTS

In the pressure range $\Delta P = P_1 \pm 25$ atm, the HWHH of both the Rayleigh line and the Brillouin line disagree with the hydrodynamic predictions of the model of Mountain and Deutch [14]. That can be seen in Fig. 5 for the Rayleigh line, where we plot the HWHH of this line for different densities. We choose the density instead of the pressure because the curves are more symmetric with that variable as quoted in the study of critical behavior of pure fluid [21]. The HWHH starts to grow for pressures higher than 40 atm corresponding to densities bigger than $\rho = 0.24$ g/cm^3 until the critical density of $\rho_C = 1.11$ g/cm^3 and decreases after this density until the density $\rho = 1.93$ g/cm^3 that corresponds to a pressure of 90 atm. We have reported the values of $D_T q^2$ in order to illustrate the different behavior of the HWHH of the Rayleigh line in this domain of pressure. This plot shows a clear perturbation centered in the critical density.

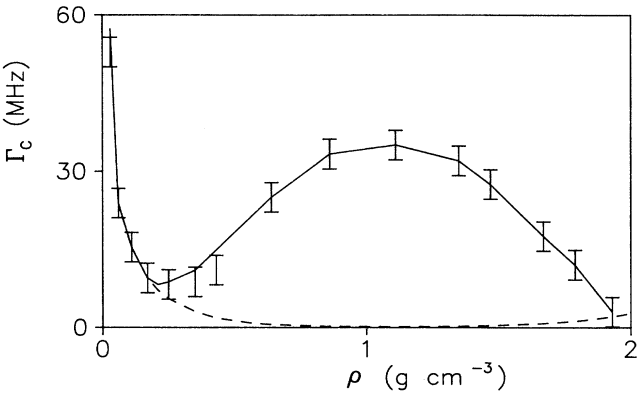

FIG. 5. Density dependence of the half width at half height (HWHH) of the central line of xenon related to the experimental diffusion coefficient D_{ex} by $\Gamma_C = D_{ex} q^2$.

The Brillouin line HWHH has a deviation too from the hydrodynamic calculation for the same density range than for the Rayleigh line. The behavior is equivalent to the Rayleigh one because this line broadens, starting from the same density until the critical density, and reduces until it reaches the hydrodynamic value. The expression of the HWHH in the hydrodynamic regime is

$$\Gamma_B = \frac{q^2}{2\rho} \left[\frac{4\eta_S}{3} + (\gamma - 1) D_T \right] \quad (1)$$

without volume viscosity term.

The increasing of the width of the Brillouin line seems, in the limits of the precision of our experimental technique, to be governed by the same expression given for the hydrodynamic regime but changing the thermodiffusivity D_T by the diffusion coefficient obtained in the Rayleigh line and shown in Fig. 5, which is called D_{ex}.

Those results are showing a different, nonhydrodynamic behavior of Γ_B and Γ_C that corresponds to different behavior of sound absorption and thermal relaxation. Those conclusions are different from the inferences of previous works and we will discuss this point in the next section.

VI. DISCUSSION AND COMPARISON WITH PREVIOUS WORKS

As said before, there are many available studies of xenon dynamics along the critical isochore, but as far as we know, it is the first time that a study along an isotherm at

high pressure is performed. In previous works, the aim was to check the validity of universal behavior of critical phenomena, but here we want to determine the dynamics at high pressure. The experimental results show a clear separation in two domains in regard to the validity of hydrodynamic calculation. Unlike previous works, we have measured the full scattered spectra and we think in terms of the full response of the fluid because we have at our disposal, simultaneously, the Rayleigh line and the Brillouin line.

Experimental previous works were effected essentially with Rayleigh-Brillouin light scattering by Cannell and Benedek [10] and Cummins and Swinney [19]; using light-beating spectroscopy by Henry, Swinney, and Cummins [13] and Eden and Swinney [22] and finally by ultrasound absorption by Garland, Eden, and Mistura and Garland, Eden, and Thoen [23].

It appears in Fig. 5 that the Rayleigh line is broadened when the density grows and approaches the critical density. That experimental fact seems to confirm the prediction of Cannell and Benedek when they talk about a "previously undetected diffusive mode" [10]. This mode is effectively a diffusive mode in the sense that it depends on the wave vector q as $D_{ex}q^2$. The new point here is that unlike Cannell and Benedek, who had obtained a spectra with an unresolved part of roughly 300 MHz centered at zero frequency, we have obtained the spectra for all frequencies of the FSR. Unlike those authors, we determine the full spectra that seem to be characterized by a HWHH much more important than the expected hydrodynamic value corresponding to the thermal diffusivity and specific heat at constant pressure contributions determined independently.

If we examine with some attention the situation at ρ_C, the common experimental condition with previous works, it is possible to check the validity of the modification of the hydrodynamic model proposed by Cannell and Benedek, in regard to our full knowledge of the spectra. Those authors introduce in the hydrodynamic equations a frequency-dependent bulk viscosity that changes the spectra by an increasing of the width of the Brillouin line and the appearance of a new central mode, named, after the author of this kind of modification, the Mountain

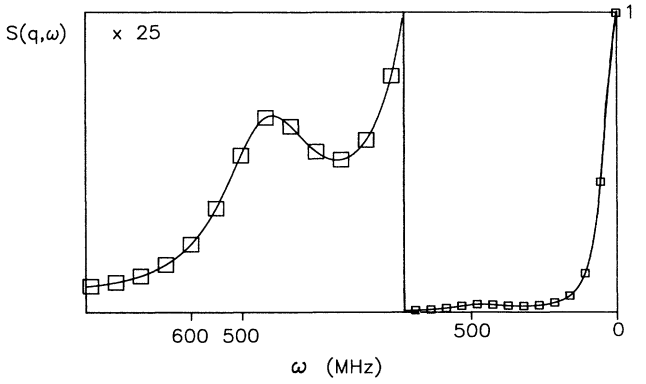

FIG. 6. Dynamic structure factor of xenon at $P=61.6$ atm. The right side corresponds to the half free spectral range and the left side is 25 times the Brillouin zone. Squares correspond to experimental points and the straight line represents the apparatus function convolved calculated spectra. See text for more details.

mode. Unhappily the amount of intensity of this mode is weak in regard to the total intensity, and the width of the Rayleigh line continues to be controlled by the thermal diffusivity $D_T=\lambda/\rho C_P$. We have evaluated numerically with the values given in [10], the spectrum corresponding to $T-T_c=3.0$ K and convolved by our apparatus function, the Cannell and Benedek calculation. The result of this calculation shows a very similar shape to the brillouin line shape we had obtained at $T-T_c=3.45$ K for the resolved part of the spectral of those authors. But if we develop the calculation for the full spectra, the calculated HWHH is too sharp in relation to the measured line. It is possible that there is only an accidental coincidence in this region of the spectra when this calculation is applied and an overlapping of Fabry-Pérot orders in the half FSR region can take place. We think that, as can be seen in Fig. 6, the Brillouin line is probably situated in the "wing" of the central line. That situation is in agreement with the important value of the Rayleigh-Brillouin intensity ratio. In Table II, we give the parameters used in the numerical simulation that describe the

TABLE II. Parameters used in the numerical simulation of the Rayleigh-Brillouin spectra. For more details see the text.

P (atm)	ρ (g cm^{-3})	D_Tq^2 (MHz)	$D_\eta q^2$ (MHz)	$\gamma-1$	$(\gamma-1)D_{ex}q^2/2$	Γ_B (MHz)	ω_B (MHz)
40.99	0.25	5.57	3.56	1.12	4.9	8.5	442
50.36	0.35	3.053	2.75	1.99	10.95	13.7	441
55.18	0.43	2.028	2.57	3.42	23.94	27.0	437
61.06	0.64	0.565	2.12	13.92	174.0	176.0	446
63.0	0.86	0.253	2.0	35.07	583.9	590.0	440
64.0	1.11	0.190	2.098	53.0	927.5	930.0	402
65.0	1.35	0.254	2.336	31.16	496.0	498.0	464
66.1	1.47	0.365	2.502	21.4	288.8	291.0	512
69.93	1.67	0.757	2.85	11.34	96.25	99.0	644
75.51	1.79	1.249	3.10	7.17	43.2	46.0	770
80.17	1.90	1.579	3.241	5.83	33.0	36.0	827
85.54	1.90	1.952	3.36	4.53	24.1	27.0	908
89.6	1.93	2.142	3.44	4.04	6.0	10.0	936

experimental spectra. For this purpose we evaluate $D_T q^2=(\lambda/\rho C_P)q^2$, $D_\eta q^2=(4\eta/3\rho)q^2$, $(\gamma-1)D_{\rm ex}q^2$, and the value of $\Gamma_B q^2$ given by formula (1) using $D_{\rm ex}$. With the values of ω_B and $\gamma-1$, we proceed to a simulation of a spectrum with a central Lorentzian governed by $D_{\rm ex}q^2$ and a shifted Lorentzian governed by Γ_B evaluated with the help of formula (1). After convolution by the experimental apparatus function, we find satisfactory agreement with the full experimental Rayleigh-Brillouin spectrum. We recall that outside the domain ΔP, $D_{\rm ex}$ coincides with D_T.

The Brillouin line, studied by many techniques along ρ_C, presents for us a nonhydrodynamic behavior in the meaning that its HWHH is much broader than the expected hydrodynamic value. We find that the HWHH increases with the density until ρ_C and decreases until it again reaches the hydrodynamic value. It is important to discuss the assumption of the introduction of a partially relaxing bulk viscosity, in order to take into account the broadening of the Brillouin line and the apparition of the new diffusive mode.

In the definition of the bulk viscosity given by Hirshfelder, Curtiss, and Bird [24], we can see that this transport coefficient can be introduced as a contribution of a polyatomic gas or a dense gas. Xenon is a monatomic gas and we cannot expect any contribution from internal degrees of freedom. For the density origin of the bulk viscosity for high density monatomic gases, as far as we know, there are measurements effected for argon at $-38.6\,^\circ$C for densities contained between 0.508 and 1.008 g/cm^3 [25]. In this work, the bulk viscosity is supposed to increase with the square of the density for all of the studied density range. Instead of this constant increase with the density and according to the behavior of the Brillouin line, the bulk viscosity should increase until ρ_C and decrease after that density. This contradiction permits us to suppose that the physical argument of bulk viscosity is not adapted for the explanation of the Brillouin width change.

In a paper devoted to the analysis of sound propagation in xenon near the critical point, Sarid and Cannell [11], after discussion of Kawasaki theory [26] and Mistura theory [27], claim that "neither theory is found to be capable of accounting for the data." Another important comment of this paper is that "not in agreement with the theory," using a frequency-dependent viscosity, the Brillouin simulations are in excellent agreement with experimental results observed near the critical point.

We try to use Kawasaki mode-coupling theory results for the hydrodynamic region ($q\xi \ll 1$) and the intermediate region ($q\xi \leq 1$), but we cannot explain our Brillouin results in the framework of that theory. It is reasonable to conclude that none of the models discussed by that author can explain our Brillouin experimental results. Otherwise our assumption that if we have a Rayleigh HWHH of $D_{\rm ex}q^2$, the Brillouin line is governed by a HWHH of the form of Eq. (1) where $D_{\rm ex}$ replaces D_T in order to have a diffusive mode due to the critical-point proximity, seems quite correct.

In the ultrasound measurements, the determination of the sound absorption seems to provide that there is no other relaxation process that disturbs the measurements, and if they exist, the data analysis can give different conclusions.

If we continue with our hypothesis, logically we have to report the problem of the interpretation of the Brillouin line to the understanding of the central diffusive mode discussed, but before that we have to give some comments about the Rayleigh measurements of xenon by LBS. In their measurements of the central line, Swinney and Henry [9] report measurements along the critical isochore for differences with critical temperature ΔT up to 5.836 K (Table I of Ref. [9]). It seems that their experimental values in the range of upper temperature difference are modified with the use of a pulse correlator and the frequency values obtained with that higher-performance apparatus are roughly 20% bigger than the previous ones. The width of the diffusive mode we find cannot be studied by the kind of correlators used by those authors; the characteristic time corresponding to the HWHH of roughly a few nanoseconds is too small and outside the correlator resolution.

Henry and Swinney say that the agreement with pulse correlator is still valid for $\Delta T < 2.5$ K but our study was held for $\Delta T = 3.45$ K, outside this region of agreement. Those bigger frequencies correspond to values of the correlation time close to the microsecond, that correspond to the lowest time resolution obtained, as far as we know, during this period, with pulse correlators. We have a free detectable stray light cell and we cannot reasonably attribute the extra scattered light to the cell-wall-scattering problem like Swinney and Henry [9]. The good accordance in the Landau-Placzek ratio evaluation seems to ensure us a free stray light situation and as quoted by Sengers and Levelt Sengers [21] there are no gravity effects in our experimental situations.

There are available Brillouin measurements performed by LBS technique by Eden and Swinney [22] in the vapor side of the coexistence curve but it is difficult for us to evaluate the resolution and the background in those experiments and we cannot discuss them. If we introduce the definition of the central line as $\Gamma_C q^2$, with the usual division into background part and critical part [4] it is possible to define Γ_C as

$$\Gamma_C = \Gamma^B + \Gamma^C , \tag{2}$$

the sum of a background part and a critical part. If, as reported by Swinney and Henry, we can define the background part as

$$\Gamma^B = \frac{\lambda^B}{\rho C_P}(1+q^2\xi^2)$$

and λ^B, ρ, and C_P are known quantities leaving a too small coefficient of diffusivity, the term contained in the parentheses cannot give any correction factor in order to understand both the central and shifted line of the spectra. The critical contribution has the following expression derived by Kawasaki:

TABLE III. Virial coefficients and their first and second derivatives as defined in text.

	$i=1$	$i=2$	$i=3$	$i=4$	$i=5$	$i=6$	$i=7$	$i=8$	$i=9$
K_i	1	0.868 602 2	−8.657 348	18.372 92	−20.556 42	13.640 28	−5.373 269	1.155 839	−0.103 346 7
K_i'	0	−0.654 594 7	9.855 160	−11.784 02	2.239 683	3.699 924	−2.324 381	0.460 604 9	−0.22 924 39
K_i''	0	2.701 269	−87.611 65	426.498 7	−1021.943	1260.016	−810.086 5	258.544 4	−32.377 97

$$\Gamma^C=\frac{k_B T}{6\pi\eta_S\xi^3}K_0(q\xi)$$

where the couplings between the different hydrodynamic modes near the critical point are taken into account. That expression was obtained using the Orstein-Zernike formula and the Kawasaki formula is

$$K_0(q\xi)=\tfrac{3}{4}[1+x^2+\langle x^3-x^{-1}\rangle\arctan x]$$

with $x=q\xi$.

Using the numerical values corresponding to $\rho=\rho_C$, $T=T_1$, $\eta_S=525$ μP, and $\xi=32.6$ Å a value of Γ_C of 0.1 MHz is obtained. This value is smaller than the expected 35 MHz obtained in our experience. For the determination of ξ, we use the relation $\xi=\xi_0[(T_1-T_c)/T_c]^{-0.63}$ with $\xi_0=2$ Å but we are not sure of the validity of this expression in the proximity of the critical point corresponding to our results. As can be seen in Eq. (2), the correlation length ξ plays crucial role in the evaluation of Γ^C and a decrease of ξ_0 allows us to approach the experimental value of $D_{\rm ex}$ a little more closely. Unhappily we do not have more physical reasons than the validity of the determination of ξ and we cannot give a satisfactory explanation of the diffusive mode fully determined in this work. Another way for the interpretation of the central width is the correction of Fixman as pointed out in [13] where Γ^B has a correction factor $1+bq^2\xi^2$ where the factor b is in general taken equal to one. We have no reasons to take b as a free parameter in order to fit the experimental results.

For further explanation of that experimental result, we think that a simultaneous study of the central line by LBS and by RBS can explain if there are one or two central modes giving a contribution to the Rayleigh line.

We believe that the physical situation corresponds to the so-called "intermediate region" where the coupling between the modes can produce the physical situations we find in our study. A further theoretical analysis of that experimental result is not easy but has to be done in order to have a clearer physical explanation.

ACKNOWLEDGMENT

Centre de Physique Moléculaire Optique et Hertzienne is "Unité Associée au Centre National de la Recherche Scientifique No. 283."

APPENDIX

The expression of the equation of state is

$$P(\rho)=\rho RT(K_1+K_2\rho+K_3\rho^2+K_4\rho^3+K_5\rho^4+K_6\rho^5+K_7\rho^6+K_8\rho^7+K_9\rho^8)\ ,$$

and the values obtained for the virial coefficients are given in Table III. Those coefficients correspond to densities expressed in g cm^{-3}.

Expressions of partial thermodynamic derivative are

$$\left[\frac{\partial P}{\partial T}\right]_\rho(\rho)=\rho R\sum_{i=1}^{9}(K_i+K_i')\rho^{i-1}\ ,$$

$$\left[\frac{\partial^2 P}{\partial T^2}\right]_\rho(\rho)=\frac{\rho R}{T}\sum_{i=1}^{9}(2K_i'+K_i'')\rho^{i-1}\ ;$$

and the expressions of C_P and C_P-C_V are

$$C_V-C_V^0=-R\sum_{i=2}^{9}\frac{(2K_i'+K_i'')\rho^{i-1}}{(i-1)}$$

and

$$C_P-C_V=R\left[\frac{\sum_{i=2}^{9}[(K_i+K_i')\rho^{i-1}]^2}{\sum_{i=1}^{9}iK_i\rho^{i-1}}\right]\ .$$

[1] P. Lallemand, J. Phys. (Paris) **32**, 551 (1970).
[2] T. G. Greytak and G. Benedek, Phys. Rev. Lett. **17**, 179 (1966).
[3] B. Y. Baharudin, P. E. Shoen, and D. A. Jackson, Phys. Lett. **42A**, 77 (1972).
[4] Q. H. Lao, P. E. Shoen, B. Chu, and D. A. Jackson, J. Chem. Phys. **64**, 5013 (1976).
[5] N. A. Clark, Phys. Rev. A **12**, 2092 (1975).
[6] L. Letamendia, J. P. Chabrat, G. Nouchi, J. Rouch, C. Vaucamps, and S. H. Chen, Phys. Rev. A **24**, 1574 (1981).
[7] G. H. Wegdam and H. M. Schaink, Phys. Rev. A **40**, 7301 (1989).
[8] S. Ranganatan and S. Yip, Phys. Fluids **9**, 372 (1966); C. D. Boley and S. Yip, *ibid.* **15**, 1424 (1972); **15**, 1433 (1972); L. Letamendia, G. Nouchi, and S. Yip, Phys. Rev. A **32**, 1082 (1985).
[9] H. L. Swinney and D. L. Henry, Phys. Rev. A **8**, 2586 (1973).
[10] D. S. Cannell and G. B. Benedek, Phys. Rev. Lett. **25**, 1157 (1970).

[11] D. Sarid and D. S. Cannell, Phys. Rev. A **15**, 735 (1977).
[12] B. J. Berne and R. Pecora, *Dynamic Light Scattering* (Wiley, New York, 1976); J. P. Boon and S. Yip, *Molecular Hydrodynamics* (McGraw-Hill, New York, 1980).
[13] D. L. Henry, H. L. Swinney, and H. Z. Cummins, Phys. Rev. Lett. **25**, 1170 (1970).
[14] R. D. Mountain and J. M. Deutch, J. Chem. Phys. **50**, 1103 (1969); C. Cohen, J. H. W. Sutherland, and J. M. Deutch, Phys. Chem. Liq. **2**, 213 (1971).
[15] H. J. Strumpf, A. F. Collins, and C. J. Pings, J. Chem. Phys. **60**, 3109 (1974).
[16] N.J. Trappeniers, *Proceedings of the Eighth Symposium of Thermophysical Properties,* edited by J. V. Sengers (American Society of Mechanical Engineers, New York, 1982), Vol. 1, p. 232.
[17] H. W. Habgood and W. G. Schneider, Can. J. Chem. **32**, 98 (1954).
[18] A. Michels, T. Wassenaar, and P. Louwerse, Physica **20**, 99 (1954).
[19] H. Z. Cummins and H. L. Swinney, Phys. Rev. Lett. **25**, 1165 (1970).
[20] J. Plantard, Memoire d'Ingenieur, Consevatoire Nation des Arts et Metier, Bordeaux, 1983.
[21] J. V. Sengers and J. M. H. Levelt Sengers, in *Progress in Liquid Physics,* edited by C. A. Croxton (Wiley, New York, 1978) Vol. 103.
[22] D. Eden and H. L. Swinney, Opt. Commun. **10**, 191 (1974).
[23] C. W. Garland, D. Eden, and L. Mistura, Phys. Rev. Lett. **25**, 1161 (1970); C. W. Garland, D. Eden, and J. Thoen, *ibid.* **28**, 726 (1972).
[24] J. O. Hirshfelder, C. F. Curtiss, and R. B. Bird, *Molecular Theory of Gases and Liquids* (Wiley, New York, 1965).
[25] W. M. Madigoski, J. Chem. Phys. **46**, 4441 (1967).
[26] K. Kawasaki, Phys. Rev. A **1**, 1750 (1970).
[27] L. Mistura, in *The Critical Phenomena,* Proceedings of the International School of Physics "Enrico Fermi," edited by S. Green (Academic, New York, 1971).